



university of
 groningen

faculty of science
 and engineering

Integration Project

Selective Laser Melting: Development of Functionally Gradient Porous Structure of SS-316L and Study of its Mechanical Behaviour for Implant Application

Alp Engin Kuvrag - S3906299

Supervisor: prof. dr. Y. (Yutao) Pei
RDP Supervisor: dr. ir. G.H. (Gerald) Jonker
Daily Supervisor: A. (Ajay) Mandal, PhD

February 2023

Abstract

Due to the increase in life pace and acceleration in population aging, millions of people suffer from bone defects caused by natural diseases and accidental injuries. As a result, bone defect treatment has become a major clinical procedure. Orthopedic designs are trying to copy the structure of bones in terms of Young's modulus, compression strength, biocompatibility, and bone ingrowth. Another aspect to be mimicked is the gradual rise in density of the bone from the inner cancellous bone to the outer cortical bone. If these designs have proper pore size and porosity, sufficient room for cell proliferation will be provided. Selective Laser Melting (SLM), an Additive Manufacturing (AM) technique, is gaining popularity due to its advantages over conventional manufacturing methods. This paper will discuss various AM processes, with an emphasis on SLM. SLM is a Laser-based Powder Bed Fusion (L-PBF) process in which the manufactured parts usually contain pores. This paper will analyze the types of pores formed in SLM-printed Stainless Steel 316L (SS-316L) parts (manufactured at various combinations of laser power and scanning speeds), as well as determine the porosity and analyze the hardness of the manufactured parts for implant applications. Functionally Gradient Porous (FGP) structures will be manufactured to mimic the human bone structure using a novel method of combining different processing parameters in a single component. This research provides valuable insight into the application of SLM for the fabrication of porous stainless steel components and FGP structures for the implant industry or any other industry that can benefit from porous structures.

Keywords: Orthopedic Designs, Implants, Additive Manufacturing (AM), Selective Laser Melting (SLM), Laser-based Powder Bed Fusion (L-PBF), Stainless Steel 316L (SS-316L), Functionally Gradient Porous (FGP) Structures, Porosity, Hardness.

Table of the Contents

Abstract	1
Table of the Contents	2
List of Abbreviations	4
1 Introduction	5
2 Literature Review	7
2.1 Types of Additive Manufacturing	7
2.1.1 Material Extrusion (ME)	7
2.1.2 Material Jetting	7
2.1.3 Electron Beam Additive Manufacturing	8
2.1.4 Laser-Based Additive Manufacturing	8
2.1.5 Selective Laser Melting (SLM)	8
2.2 Applications of SLM	9
2.2.1 Aerospace Industry	9
2.2.2 Automotive Industry	11
2.2.3 Medical Industry	11
2.3 Applications of Stainless Steel 316L	13
2.3.1 Medical Implants	13
2.3.2 Kitchen Appliances	13
2.3.3 Marine Applications	13
2.3.4 Industrial Applications	14
3 Research Scope and Objective	15
3.1 Problem Statement	15
3.2 Research Objective	15
4 Materials and Methods	17
4.1 Material Selection	17
4.1.1 Gas Atomized SS-316L	17
4.1.2 Argon Gas & Sieving	17
4.2 Sample Preparation	18
4.2.1 Samples	18
4.2.2 Metallography	20
4.3 Porosity Measurements	21
4.4 Hardness Measurements	21
4.5 Proposal of Functionally Gradient Porous Structure	22

5 Results	23
5.1 Porosity Analysis	23
5.2 Hardness Analysis	27
5.3 Functionally Gradient Porous Structure	30
6 Conclusion	31
6.1 Impact of Laser Parameters on Melting and Solidification Mechanisms	31
6.2 Proposed FGP Structure	31
6.3 Future Research	32
7 References	32

List of Abbreviations

AM - Additive Manufacturing

SLM - Selective Laser Melting

SS-316L - Stainless Steel 316L

PBF - Powder Bed Fusion

L-PBF - Laser Powder Bed Fusion

FGP - Functionally Gradient Porous

SS - Scanning Speed

LP - Laser Power

SD - Scanning Direction

BD - Building Direction

1 Introduction

Additive manufacturing (AM), commonly known as 3D printing, is a revolutionary technology that has been developed over the past few decades and is transforming the way parts are manufactured. It is the process of building a 3D object layer by layer from a digital model. This technology has existed for over 30 years, but it has only recently gained the attention of both technology experts and the general public [1]. When the last major fused deposition modeling (FDM) patent expired in 2009, printers could be produced without infringing on intellectual property, which sparked interest and investment in AM technologies [1]. This technology is becoming even more popular because it appears to point to a future in which value chains will be shorter, smaller, more localized, more collaborative, and offer major sustainability benefits [2]. Compared to conventional manufacturing methods such as machining, casting, and forging, additive manufacturing offers greater geometrical flexibility and faster production times for mass customization of products.

Conventional manufacturing processes have been used for centuries to produce parts and components. These processes are well-established and have proven to be reliable and cost-effective. However, they require extensive tooling and setup time, which can be costly and time-consuming. Additionally, conventional methods are limited in their ability to produce complex geometries, and in most cases, they require multiple secondary operations and post-processing to create the desired component. In Mohsen Attaran's work, the advantages of AM over conventional manufacturing are discussed and summarized in Table 1.

AM has several advantages over conventional manufacturing methods. It enables, for instance, the production of complex geometries directly from a digital file with minimal setup time and without the need for costly tooling. As there is no need for extensive setup time, AM can also reduce prototype development and manufacturing lead times. Moreover, additive manufacturing can reduce waste in the manufacturing process because it only uses the amount of material required to produce the part.

This paper will provide an overview of the literature on the various types of additive manufacturing, with a particular focus on Selective Laser Melting (SLM) and its applications. Applications of Stainless Steel 316L will also be covered in the literature overview. The research objectives will be outlined in Section 3.4, and the methodology for achieving these objectives will be discussed. A hypothesis will be formed in Section

4.5. After discussing the results and conclusions, further research areas will be suggested.

Table 1. Advantages of additive manufacturing over conventional manufacturing [1]

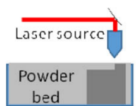
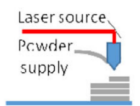
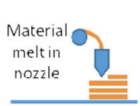
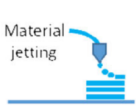
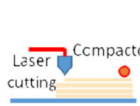
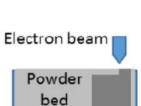
Areas of Application	Advantages
Rapid Prototyping	Reduce time to market by accelerating prototyping Reduce the cost involved in product development Making companies more efficient and competitive at innovation
Production of Spare Parts	Reduce repair times Reduce labor cost Avoid costly warehousing
Small Volume Manufacturing	Small batches can be produced cost-efficiently Eliminate the investment in tooling
Customized Unique Items	Enable mass customization at low cost Quick production of exact and customized replacement parts on site Eliminate penalty for redesign
Very Complex Work Pieces	Produce very complex work pieces at low cost
Machine Tool Manufacturing	Reduce labor cost Avoid costly warehousing Enables mass customization at low cost
Rapid Manufacturing	Directly manufacturing finished components Relatively inexpensive production of small numbers of parts
Component Manufacturing	Enable mass customization at low cost Improve quality Shorten supply chain Reduce the cost involved in development Help eliminate excess parts
On Site and On-Demand Manufacturing of Customized Replacement Parts	Eliminate storage and transportation costs Save money by preventing downtimes Reduces repair costs considerably Shorten supply chain The need for large inventory is reduced Allow product lifecycle leverage
Rapid Repair	Significant reduction in repair time Opportunity to modify repaired components to the latest design

2 Literature Review

2.1 Types of Additive Manufacturing

Currently, various types of AM processes are commercially available to fabricate components from different materials, such as polymer, metal, and ceramic. On the basis of type of material and deposition mechanism, H. Bikas et al. classified the AM processes into five different categories: Laser Based, Extrusion Thermal, Material Jetting, Material Adhesion, Electron Beam. The schematic representations, names of the sub-categories, and types of material used in these processes are listed in Table 2 [3].

Table 2. Additive manufacturing process categorization showing the schematic representations, names of the sub-categories, and types of material used [3].

Additive Manufacturing (AM) Processes														
Process	Laser Based AM Processes				Extrusion Thermal	Material Jetting	Material Adhesion	Electron Beam						
	Laser Melting		Laser Polymerization											
Process Schematic														
Name Material	SLS	Green	DMD	Green	SLA	Blue	FDM	Red	3DP	Green	LOM	Red	EBM	Green
	SLM	Green	LENS	Green	SGC	Blue	Robocasting	Red	IJP	Blue	SFP	Red		
	DMLS	Green	SLC	Green	LTP	Blue			MJM	Blue				
			LPD	Green	BIS	Blue			BPM	Blue				
					HIS	Blue			Ther Mojojet	Blue				
Bulk Material Type		Powder	Green	Liquid	Blue	Solid	Red							

2.1.1 Material Extrusion (ME)

ME is the layer-by-layer deposition of molten material through a nozzle. In most ME systems, feedstock material is extruded through a nozzle's orifice and melted by a resistive heating system. The extrusion head is moved by a gantry in the x and y directions to selectively dispense material onto a pre-heated platform. Once a full slice is printed, the nozzle is moved away from the last printed layer along the z-axis to print the next slice. This process is repeated until the part is finished [4].

2.1.2 Material Jetting

Material Jetting AM, also known as inkjet 3D printing, is an established AM process that creates parts by depositing droplets of liquid photopolymers using piezo printing heads and curing them with ultraviolet lamps. Inkjet 3D printers such as

Stratasys' PolyJet and 3D Systems' MultiJet can deposit multiple photo-curable polymer resins simultaneously to manufacture multi-material parts [5].

2.1.3 Electron Beam Additive Manufacturing

EBAM is a relatively new technology that can produce metallic components layer by layer. This process uses a high-energy electron beam as a moving heat source to melt metallic powders, fuse them together by rapid self-cooling, and create packed-density functional metallic components [6]. It is important to note that this process is carried out in a vacuum environment [6], eliminating the need for argon or any other inert gas compared to Laser-Based Additive Manufacturing.

2.1.4 Laser-Based Additive Manufacturing

Laser-based AM processes are very similar to the EBAM process, in which instead of an electron beam, a high-energy laser is used to selectively melt and fuse metal powder. Both of these processes are powder bed fusion (PBF) processes in which gas-atomized metal powder is uniformly spread over the build platform, which is then melted selectively using an electron beam or high-power laser source according to the 3D CAD model of the component. This study is going to focus on selective laser melting (SLM), which is a laser powder bed fusion process (L-PBF).

2.1.5 Selective Laser Melting (SLM)

SLM is one of the major AM technologies that has been used for a variety of applications in the aerospace, automotive, defense, and medical industries. It provides the flexibility to process wide variety of metals and alloys such as, Ti6Al4V, β -type Ti-24Nb-4Zr-8Sn, Ni superalloy, and 316L stainless steel [7]. The laser beam is used to completely melt the aforementioned metal powder layers spread on a powder bed to form near-net-shaped components by slicing 3D models into 2D layers with specified thickness values [8]. The molten powder particles then resolidify and fuse together to form the desired shape. This layer-by-layer deposition process is repeated until the desired geometry is achieved [9]. Figure 1 displays a schematic representation of SLM.

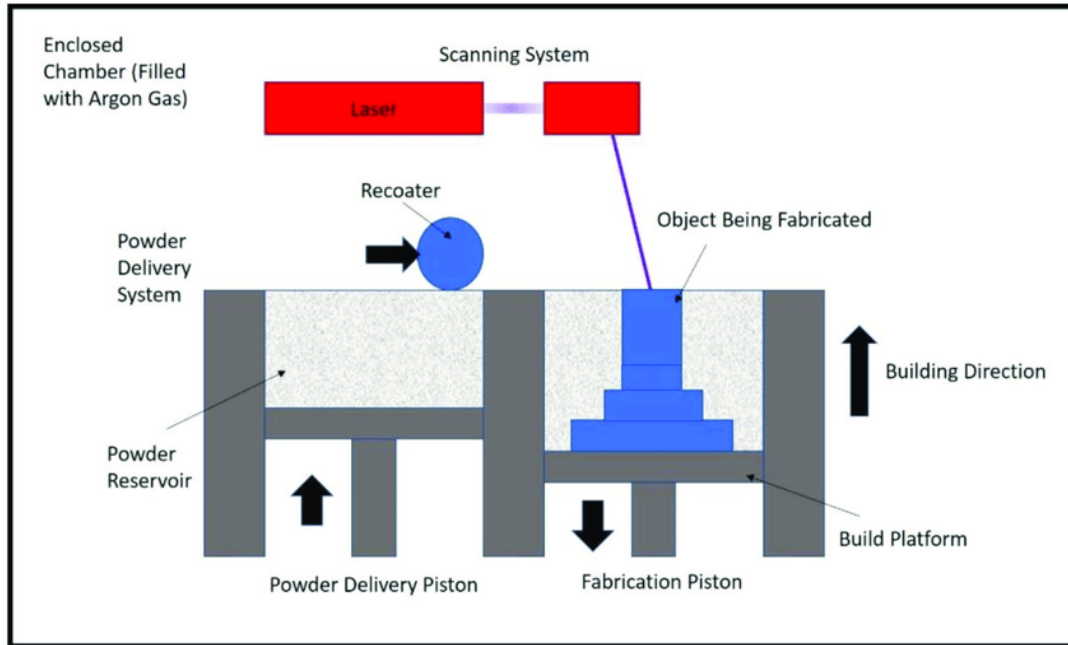


Figure 1. Schematic representation of the SLM process [10].

2.2 Applications of SLM

These days, the development of complicated porous structures through L-PBF is an interesting topic of research for the scientists. Utilizing this technology, researchers and manufacturers have created a variety of porous structures with distinct properties and applications. Although the porosity of SLM parts processed with optimized parameters does not significantly reduce the load bearing area and may therefore not be sufficient to reduce the stiffness of the material in load bearing applications [11], this is not the case for fatigue performance, which is strongly influenced by the presence of pores [12]. Since fatigue cracks initiate at these defects, the probability of failure under cyclic loading rises as their proportion or size increases [13], which is an essential consideration for application domains.

2.2.1 Aerospace Industry

SLM technology is gaining increasing traction in the aerospace industry due to its capacity to manufacture complex components with a high degree of accuracy and repeatability [14]. Using this technology, high-value components with complex internal structures that would be difficult to produce using conventional methods have been manufactured. For instance, the part depicted in Figure 2 can not be produced using the conventional methods such as cutting, milling, or grinding.



Figure 2. As manufactured high-value aerospace component [14]

Additionally, SLM technology has been utilized to manufacture lightweight components with superior mechanical properties. This has made it possible to produce lighter, more fuel-efficient aircraft. M. Seabra et al. [15] attempted to achieve this in their work by utilizing SLM and topology optimization to manufacture an aircraft component. In conclusion, the material volume is reduced by 54%, resulting in a 28% weight reduction. The smaller reduction in weight is a result of the change from aluminum to titanium alloy.

Furthermore, in the work of M. Bici et al. [16], attempts were made to develop multifunctional aerospace panels. Figure 3 depicts the panel's structure. This new patent-protected system employs a lattice core as a heat exchanger, which is covered by plates, and the entire structure is produced in a single SLM process. Using this sandwich, a light and rigid structure with a large internal thermal exchange surface can be created.

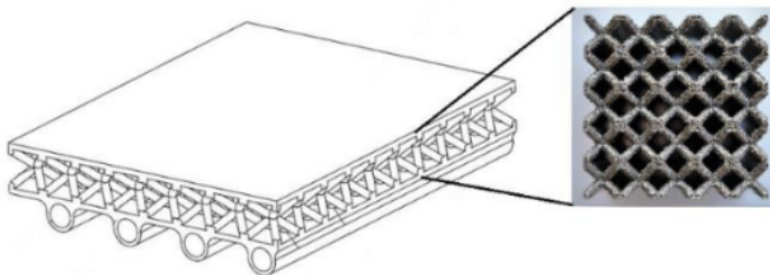


Figure 3. Panel section with focus on the lattice core [N8, 16].

2.2.2 Automotive Industry

The automotive industry has also recognized the potential of SLM technology in the production of complex geometries while maintaining relative strengths [17]. This technology has been used to produce parts with complex geometries, such as engine components, exhaust systems, and brake rotors, that would be difficult to produce using conventional methods [18]. In addition, SLM technology has been utilized to produce parts with superior mechanical properties, allowing for the production of lighter, more fuel-efficient vehicles [18].

For instance, J. Piekło and A. Garbacz-Klempka designed and manufactured an aluminum alloy steering gear housing using SLM instead of pressure die casting. The CAD model and the SLM part of the housing are shown in Figure 4.

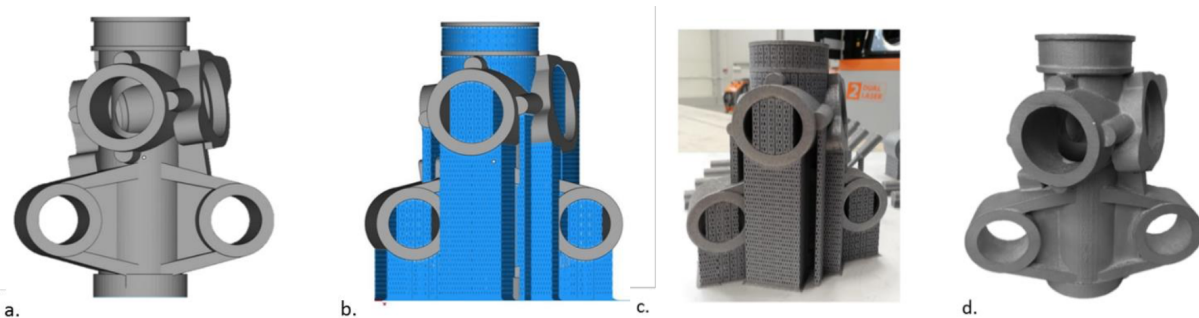


Figure 4. CAD model and SLM part of the automotive steering gear housing: a. CAD model of the gear housing; b. CAD model of the gear housing with added support structures; c. the gear housing with support structures fabricated using the SLM method; d. cleaned gear housing fabricated using the SLM method [19].

2.2.3 Medical Industry

The potential of SLM technology for the creation of components with superior mechanical properties for use in implant applications has been recognized by the medical sector. For instance, it is explained in the work of S. Ferrais and S. Spriano that AM processes, primarily LPBF ones, are gaining popularity for the creation of specifically designed porous titanium constructs for biomedical applications, particularly for bone replacement. It also goes over how modifying the surface of AM constructs can alter their biological response, enhance bone bonding, and increase bacterial resistance [20].

Moreover, the work of A. Gebhardt et al. indicates that, after the 2009 introduction of desktop SLM machines, small companies that require tiny,

custom-designed components began utilizing SLM technology. Consequently, businesses engaged in crafts, such as dental laboratories, were the primary targets. They investigated the possibility of SLM delivering a dense, custom-made, three-piece demonstrator bridge during their research. Figure 5 depicts the printed and manually finished component. They asserted that after manual work, the part's surface quality was excellent, and microscopic examination confirmed its density and lack of pores [21].



Figure 5. SLM-printed three-piece demonstrator bridge after manual surface finishing [21].

As mentioned in Section 2.2, “Applications of SLM”, defects such as pores and cracks increase the likelihood that SLM parts will fail under cyclic loading. To determine the suitability of SLM for high performance and dynamic applications in the medical industry, E. Wycisk et al. conducted exploratory research in which they conducted high cycle fatigue (HCF) tests on as-built, polished, and shot-peened samples. As a result of the poor surface quality produced by the SLM process, as built samples demonstrated a significant decrease in fatigue limit. In addition, polishing increased the fatigue limit to greater than 500 MPa, which is the average value for base material. However, shot-peening proved to have the opposite effect than anticipated and decreased the fatigue limit drastically [22].

Overall, SLM technology is becoming more popular in a wide range of industries. This technology has proven to be a viable option for producing complex components in numerous industries, including aerospace, automotive, and medicine. Despite the fact that the presence of pores and other flaws may limit the use of SLM in certain applications, the benefits associated with this technology make it a viable option for many applications.

2.3 Applications of Stainless Steel 316L

Stainless steel 316L is an alloy consisting of iron, chromium, nickel, molybdenum, and manganese. It is an extremely corrosion-resistant version of stainless steel grade 316 with a low carbon content [23]. The high molybdenum content provides excellent resistance to pitting and crevice corrosion [23]. Furthermore, the high content of chromium will form a chromium oxide layer, which will act as a protective layer and protect the surface from further corrosion [24]. It is employed in a vast array of applications, including medical implants, kitchen appliances, marine applications, and industrial applications.

2.3.1 Medical Implants

Due to its superior corrosion resistance, biocompatibility, and strength, stainless steel 316L is widely used for medical implants. It is one of the preferred materials for implants requiring durability, such as hip and knee replacements [25]. In addition, when nickel is removed and nitrogen content is increased, SS-316L's wear resistance increases, making it an even better material for load-bearing implants such as joint replacements [26]. Moreover, it is used for dental implants, though for long-term use, surface modifications can be necessary due to the moist environment [27].

2.3.2 Kitchen Appliances

SS-316L is a popular choice for kitchen appliances due to its attractive appearance and superior corrosion resistance. Because it is highly corrosion-resistant and can withstand high temperatures, the material is utilized in range hoods, dishwashers, cooktops, ovens, and kitchen sinks [28]. Additionally, the material is easy to maintain and clean, and it can be sterilized without deterioration [29], making it a viable material for utensils.

2.3.3 Marine Applications

Due to its superior corrosion resistance, SS-316L is widely employed in seawater environments and referred to as "marine grade stainless steel" in the industry. Numerous components of cooling water systems, including heat exchangers, piping, and water jackets, are made of stainless steel [30]. In recent years, the material has also become a common tank material. By improving the chemical resistance of the material

and designing it so that it can be cleaned and inspected, contamination risks in cargo can be easily mitigated [31].

2.3.4 Industrial Applications

A wide variety of industrial applications make use of austenitic stainless steel 316L due to its high strength, high resistance to heat, and good weldability [24]. Among these applications are heat exchangers, dyeing equipment, film processing equipment, pipelines, etc. [32]. Because of its exceptional resistance to corrosion and oxidation, it is also widely used as an important industrial alloy in work done in the nuclear field at high temperatures [33]. In spite of the fact that the material can be utilized as an exterior construction material in coastal areas [32], its structural applications are constrained due to its relatively low strength in comparison to other comparable materials used in the field [33].

In conclusion, stainless steel 316L is a highly versatile material with numerous applications. Its corrosion resistance and durability make it a perfect choice for medical implants, kitchen appliances, and a variety of components in cooling water systems. It is also utilized in nuclear fields and coastal areas due to its resistance to oxidation and corrosion. Its low strength, however, limits its use in structural applications.

3 Research Scope and Objective

Even though AM has the potential to revolutionize the design and manufacture of products, there are still a number of research gaps that must be filled before it can reach its full potential. For instance, the development of gradient porous structures through LPBF is still a challenging task for researchers. Furthermore, the mechanical behavior of gradient porous structures having random pore distribution geometry is unclear in the scientific domain. This type of structure has great application in implant development, and therefore it needs to be explored extensively.

3.1 Problem Statement

This research arises from the need to create functionally gradient porous (FGP) structures, as these structures can benefit a considerable number of fields. However, the emphasis will be on implant applications. Conventional manufacturing methods restrict the current state of the art in implant production. Different patients have different physical characteristics, necessitating the need for custom implants that fit different body types. However, custom implants cannot be easily produced using conventional manufacturing techniques as they require design and/or material-dependent tooling (e.g., jigs and fixtures) [34]. In addition, conventional manufacturing techniques struggle to generate porosity gradients within the implant structure, which would otherwise provide a more favorable environment for cell proliferation and adhesion [35]. Moreover, commercially available implants manufactured with conventional techniques have a denser structure and higher stiffness than bones, which can result in stress shielding phenomena [36]. Although lattice-based porous structures are described in the literature [36], random porosity is preferred for implant structures because it resembles the bone structure more closely. Furthermore, lattice-based porous structures not only require tedious design to achieve desired porosity levels, but it is even more complex to design FGP structures.

3.2 Research Objective

This research aims to analyze the porosity morphology and fraction of SLM-manufactured samples to determine the impact of process parameters (laser power and scanning speed) on the melting and solidification mechanisms of SS-316L. Thereafter, a hardness analysis is performed on the samples manufactured at different combinations of laser power and scanning speed to determine the relationship between

porosity and hardness. The main objective is to develop a cylindrical FGP structure by adjusting the processing parameters of SLM (laser power and scanning speed) in a single component without any design requirement. Further elaboration on the development of the FGP structure is given in Section 2.5, “Functionally Gradient Porous Structure Preparation”.

4 Materials and Methods

4.1 Material Selection

4.1.1 Gas Atomized SS-316L

Recent interest in manufacturing techniques employing metal powders, such as additive manufacturing (AM), metal injection moulding (MIM), and hot isostatic pressing (HIP), has increased the demand for manufacturing alloyed metal powders, especially iron-, nickel-, and cobalt-based alloys [37]. There are a variety of methods for atomizing metal powder, including gas atomization, electrode induction gas atomization, plasma atomization, water atomization, and ultra-high pressure water atomization [37]. Inert gas atomization (IGA) is a process in which the melt is atomized with an inert gas, typically nitrogen or argon, to prevent oxidation [38].

In this study, argon gas-atomized 316L SS powder (supplied by Carpenter Additive) with particle diameters ranging from 15 to 40 μm is utilized to manufacture the samples. Table 3 shows the composition of the powder.

Table 3. SS-316L powder composition provided by Carpenter Additive [39].

Iron	Balance	Chromium	16.0–18.0 %	Nickel	10.0–14.0 %
Molybdenum	2.00–3.00 %	Manganese	2.00 %	Silicon	1.00 %
Nitrogen	0.10 %	Oxygen	0.10 %	Phosphorus	0.045 %
Carbon	0.030 %	Sulfur	0.030 %		

The low levels of phosphorus, carbon, and sulfur reduce the susceptibility of the samples to sensitization, which could otherwise lead to a reduction in the samples' mechanical properties [40].

4.1.2 Argon Gas & Sieving

Argon, the inert gas used to atomize the SS-316L, is an important part of the process as well, as the powder reservoir, the building chamber, and the sieving process of the SLM machines all utilize purity argon to minimize oxidation. After each printout, the excess powder in the building chamber is collected in a container and subjected to sieving. This needs to be done because, during the printing process, some of the powder might have coalesced due to melting, producing larger particles. To maintain the powder quality, these particles are separated from the powder with the desired particle size mentioned before (15 to 40 μm). The sieving machine also refills the containers filled with reusable powder with argon gas, once again to minimize oxidation.

4.2 Sample Preparation

4.2.1 Samples

Using the Selective Laser Melting System SLM 125HL, a set of 16 samples was manufactured. Each sample was made with a different combination of laser power and scanning speed. The range of laser power is 100, 200, 300, and 400 W, and the range of scanning speed is 300, 800, 1300, and 1800 mm/s. The layer thickness and hatch spacing were maintained at 30 and 108 micrometers, respectively. As the scanning method, the meander scanning strategy was used. The strategy for producing these samples is depicted in Figure 7.

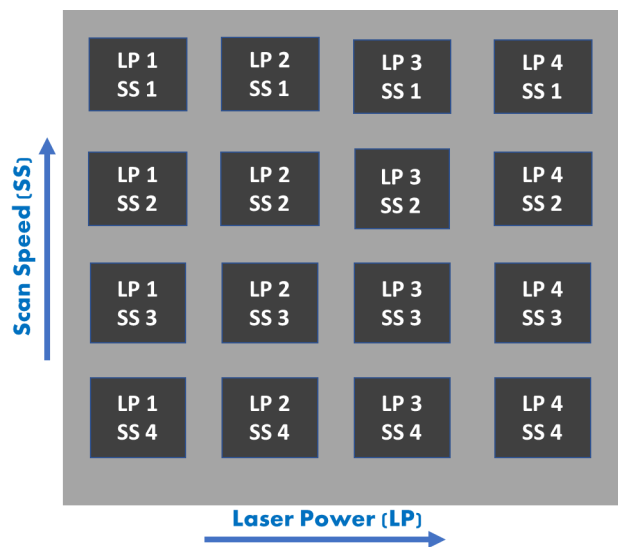


Figure 7. Schematic representation of the manufacturing strategy followed for 16 samples. Each square represents a sample, and the gray square behind the samples represents the plate that the samples will be printed on.

The printed out samples can be seen in Figure 8. These samples were sectioned into two pieces so that they can be observed and characterized from both building (BD) and scanning (SD) directions. Any surface or cross section of the samples that is perpendicular to the building platform is referred to as BD, and any surface or cross section that is parallel to the building platform is referred to as SD, which is depicted in Figure 9.



Figure 8. Substrate plate with 16 samples manufactured at different laser powers and scanning speeds.

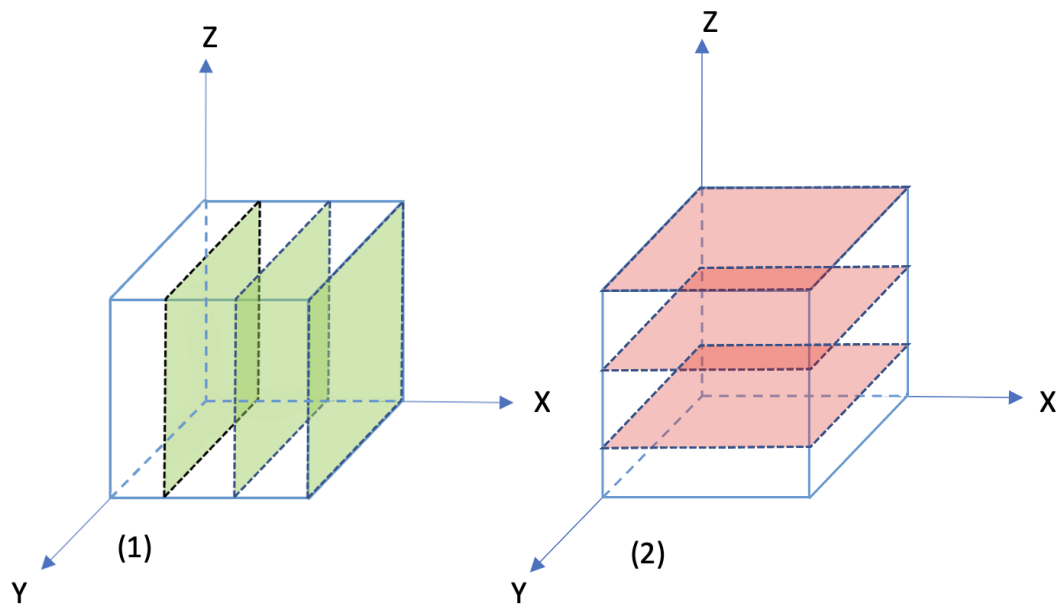


Figure 9. The X-Y plane represents the building platform. BD stands for surfaces or cross sections that are perpendicular to the building platform and are depicted in (1). SD stands for surfaces or cross sections that are parallel to the building platform and are depicted in (2).

4.2.2 Metallography

Once the samples had been cut from the substrate plate shown in Figure 8, each sample was then sectioned into two pieces. Following this, the sectioned samples were hot-mounted into epoxy resin before being subjected to a grinding and polishing process. Coarse grinding was done with 80 and 320-grade sandpapers, respectively, on a horizontal rotary surface grinder for 15–30 seconds. Time is kept short in order to minimize the material loss of the samples. Fine grinding was done with 1000, 2000, and 4000-grade sandpapers, with the grade increasing when all scratches on the surface are parallel to each other. The importance of making sure that all the scratches are parallel is to ensure that all the scratches are caused by the current sandpaper and that there are no deeper scratches. Finally, OPS solution was used to polish the samples with a polishing cloth until the surface had no scratches and reflected light like a mirror. The samples were then ready for optical analysis under an optical microscope (see Figure 10).

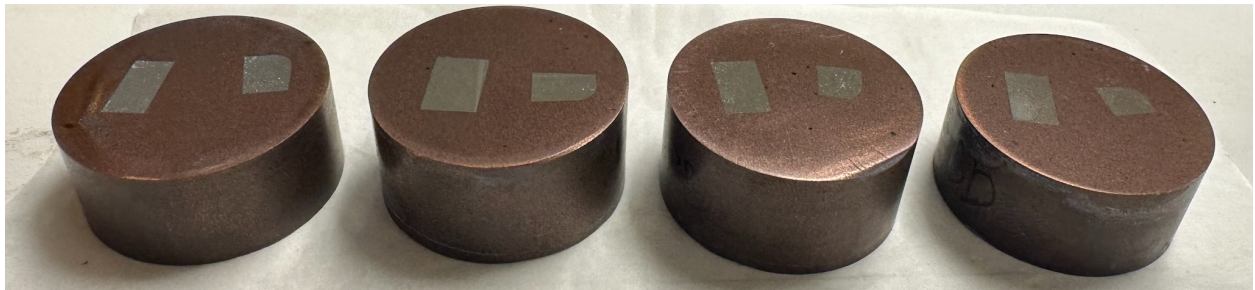


Figure 10. Polished samples for measuring porosity. The epoxy resin mounts are holding the samples from 1 to 4. The larger sectioned piece of each sample is the BD sample, while the smaller sectioned piece is the SD sample.

4.3 Porosity Measurements

In order to calculate the porosity, nine optical images for each sample are captured at a 20-x magnification. Images captured at lower magnifications did not display pores as clearly as those captured at 20x magnification. In contrast, the images captured at higher magnifications did not accurately depict the porosity of the samples, as only a very small portion of the surface was visible. The pictures are shot from the same positions for each rectangle to reduce bias and randomness, and the strategy is depicted in Figure 11. Using the image processing software ImageJ, the surface porosity and pore size fraction are then calculated.

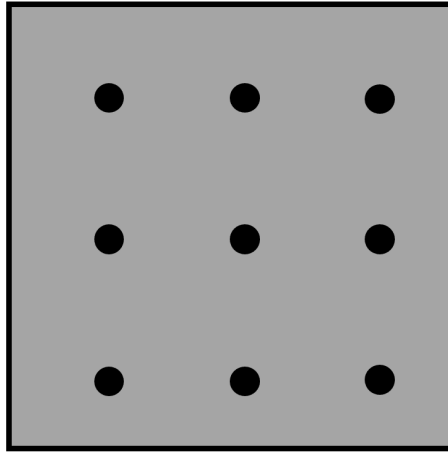


Figure 11. 2D representation of a sample surface. The black dots represent the nine locations used to take the optical microscopy images for porosity measurements.

4.4 Hardness Measurements

Vickers Hardness (HV) was used to measure the hardness of samples and the FGP structure. The LEITZ Micro Hardness Tester was employed to create and measure indentations. The resulting values were calculated using Equation (1),

$$H_V = \frac{kP}{d^2} \quad (1)$$

where k is a constant dependent on the indenter geometry and the units chosen, P is the applied load of 2.942 Newtons (300 g), and d is the average diagonal length of the indent in micrometers [41]. The units of Vickers Hardness (HV) generally correspond to kgf mm⁻², where 1 kgf mm⁻² is equivalent to 9.81 MPa [41].

4.5 Proposal of Functionally Gradient Porous Structure

Changing laser parameters in a single component to manufacture a FGP structure is an area that needs extensive research. In this study, a structure of four concentric cylinders with different laser power and scanning speed combinations is proposed to explore the feasibility of a single fused specimen. Thus, a hypothesis in the form “Concentric cylinders manufactured with different laser power and scanning speed combinations can fuse together to form a solid, properly fused structure” can be formed. The proposed structure has a diameter of 16 mm and a height of 32 mm. Figure 12 illustrates the production strategy for this structure. The same scanning method as for the individual samples, the meander scanning strategy, will be utilized.

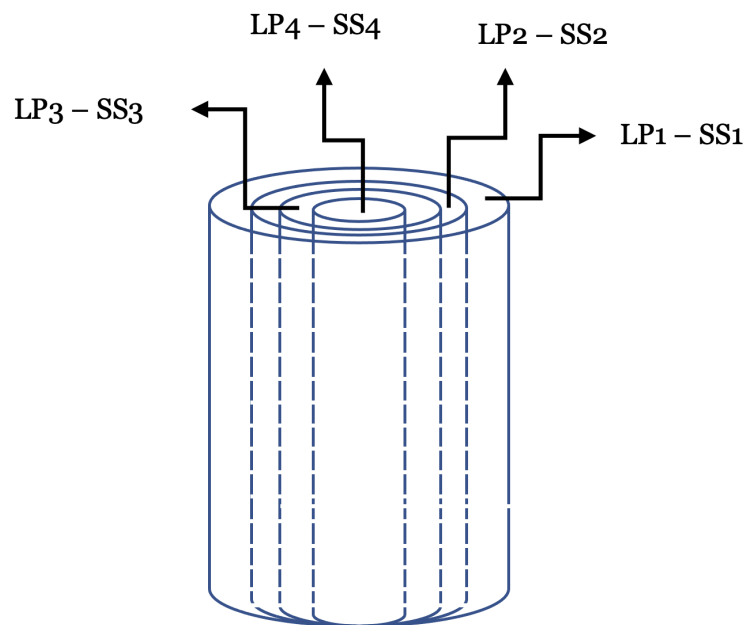


Figure 12. Schematic representation of the manufacturing strategy followed for the FGP structure.

5 Results

5.1 Porosity Analysis

Figure 13 depicts how laser power and scanning speed affect the porosity change in both scanning and building directions. The porosity along the scanning direction (SD) and the building direction (BD) follow the same pattern in both graphs. It can also be observed that the porosity has a negative correlation with the laser power and a positive correlation with the scanning speed.

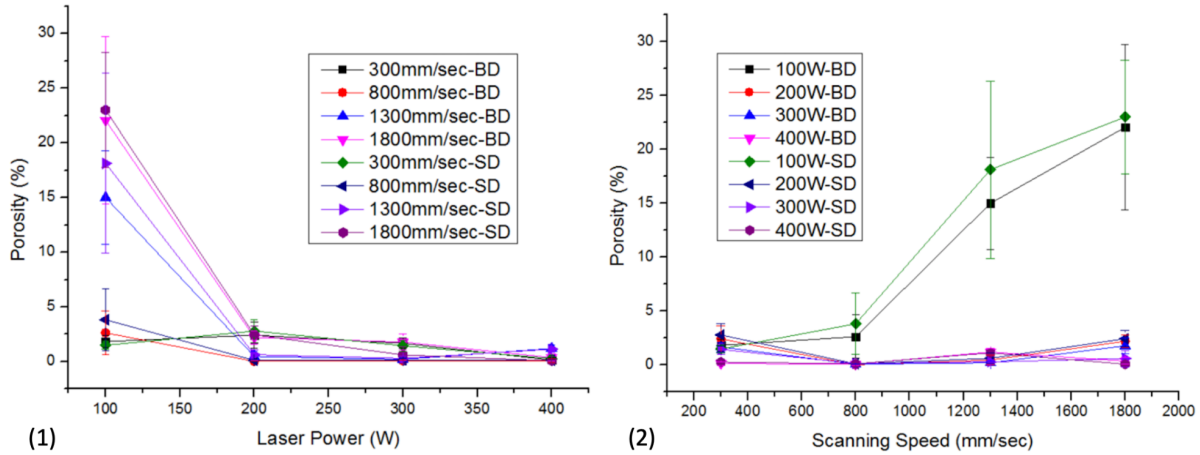


Figure 13. Change in porosity in both SD and BD as a function of (1) Laser Power and (2) scanning Speed

When the laser power is reduced to 100W at scanning speeds of 800, 1300, and 1800 mm/sec, the porosity drastically increases, especially at 1300 mm/sec and 1800 mm/sec, where the porosity reaches 18.14% and 23.03%, respectively. This is mentioned in the work of Sola and Nouri, which states that a lack of fusion results in incomplete fusion between adjacent layers and adjacent melt pools when very low laser power or excessive scanning speed is used [42]. Therefore, it can be inferred that using a low laser power and a high scanning speed will result in high porosities.

Sola and Nouri classified the types of porosity observed in laser-based SLM into four categories, as shown in Figure 14: (A) entrapped gas porosity, (B) incomplete melting-induced porosity, (C) lack of fusion with unmelted particles inside large irregular pores, and (D) cracks [42]. Incomplete melting-induced porosity, (B), will be referred to as "keyhole porosity," as in the papers of T. Wang et al. [43] and J. N. Zhu et al. [44].

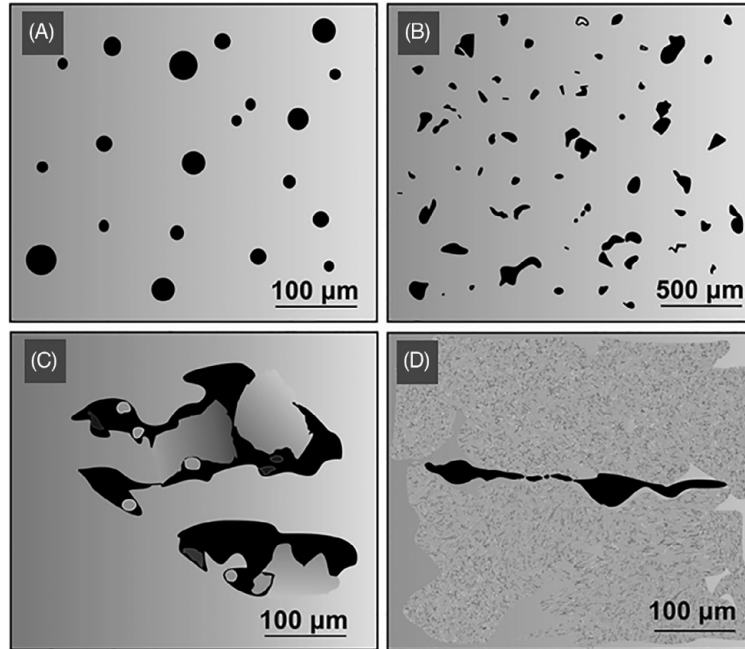


Figure 14. Types of porosity observed in samples: (A) entrapped gas porosity, (B) keyhole porosity, (C) lack of fusion with unmelted particles inside large irregular pores, and (D) cracks [42]

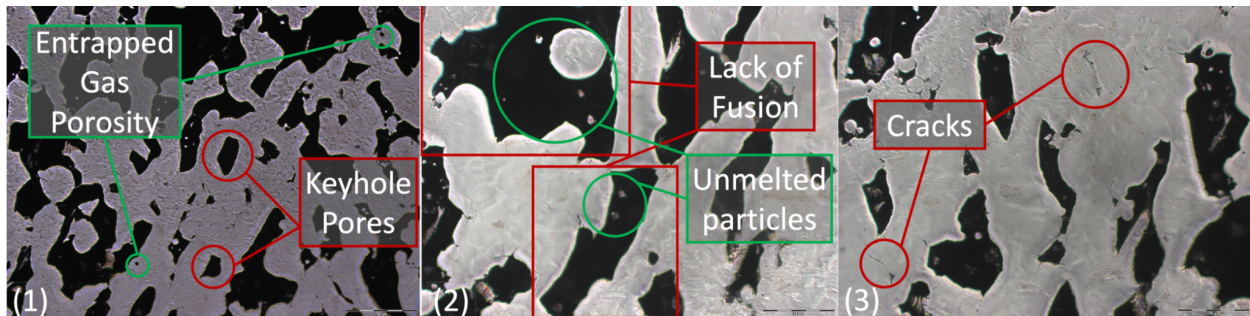


Figure 15. (1) Entrapped gas porosity and keyhole porosity at 10x magnification, (2) lack of fusion pores with unmelted particles inside large irregular pores at 20x magnification, and (3) cracks at 20x on sample 13-SD observed under optical microscopy.

Figure 15 depicts the types of pores observed on sample 13 (in scanning direction) under optical microscopy. Sample 13 had the highest porosity of all the samples in this study, at 23.03%. The majority of the defects are either keyhole pores or a lack of fusion pores. Different pores have different formation mechanisms, but the primary cause is usually the unoptimized processing parameters.

When the metal powder does not melt completely and cannot fuse to form a solid layer because the laser scans too quickly or lacks sufficient power, keyhole pores form (unoptimized processing parameters) [44]. Lack of Fusion pores occur when the Keyhole porosity formation mechanism leads to bigger pores where these pores tend to have unmelted powder particles in spherical shapes [44]. Cracks form due to the

thermal stresses [42], which are also caused by unoptimized processing parameters [44]. Entrapped Gas Porosity can occur for two different reasons: gas particles entrapped during the gas atomization of the SS-316L feedstock powder [45], and gas particles that are already in the building chamber and trapped between powder particles and layers during SLM processing [46].

Figure 16 depicts optical microscopy images at every combination of laser power and scanning speed used in this research to examine the effect of these parameters on the types and number of pores. Lack of fusion and keyhole pores were observed to form at low laser power and high scanning speed more often, as can be seen on samples 9 and 13 in the figure.

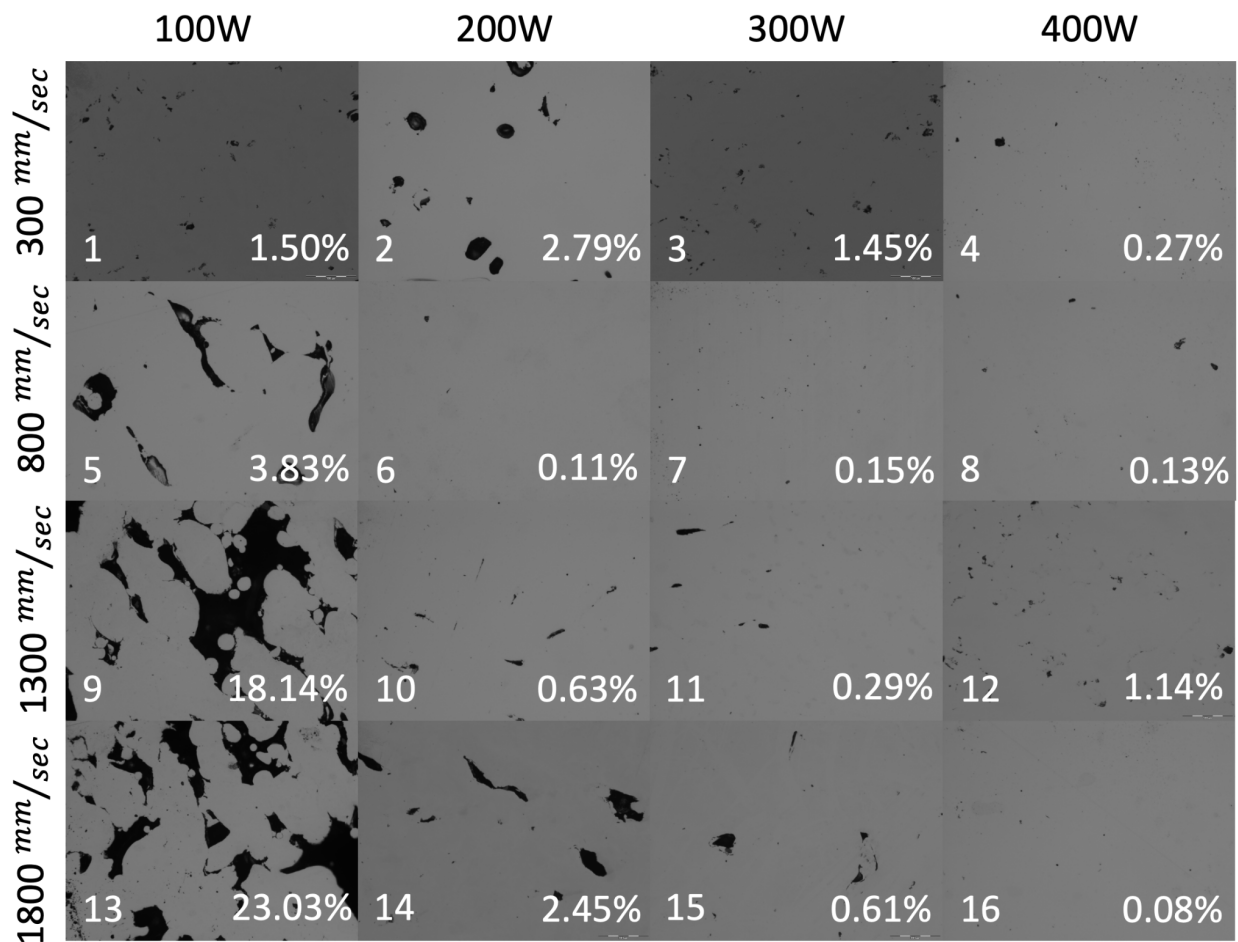


Figure 16. Optical microscopy images of the scanning direction samples at every combination of laser power and scanning speed. Sample number and percentage porosity are shown at the left and right bottom corners, respectively.

For any tissue engineering application, including implant applications, mean pore size is a crucial aspect to be considered. However, it is not easy to agree on the optimal mean pore size for implants as there is conflicting research on the aspect. The conflict arises from the fact that pores that are too small can limit cell migration, which then limits the diffusion of nutrients and the removal of waste [47]. On the other hand, if the pores are too large, it leads to weaker cell attachment [47]. Previous studies indicate that a mean pore size of 96–150 μm is optimal for cell attachment, whereas for optimal cell migration to support successful bone growth, a mean pore size of 300–800 μm is required [48]. Table 4 displays the average pore sizes of the samples characterized in the research. The mean pore sizes of samples 2, 5, 9, and 13 fall within the range of an optimal mean pore size for cell attachment and migration.

Table 4. Mean pore sizes in BD, SD, and the average mean pore size

Sample #	Mean Pore Size in BD (in μm)	Mean Pore Size in SD (in μm)	Avg. Mean Pore Size (in μm)
1	21.3	18.4	19.9
2	109.5	282.5	196.0
3	20.8	18.6	19.7
4	15.8	5.3	10.6
5	107.8	140.0	123.9
6	5.2	15.1	10.2
7	19.0	3.5	11.3
8	17.2	13.8	15.5
9	356.9	473.5	415.2
10	45.0	20.4	32.7
11	21.6	21.1	21.4
12	14.8	12.4	13.6
13	408.1	374.4	391.3
14	55.1	87.2	71.2
15	31.7	26.0	28.9
16	23.2	4.9	14.1

5.2 Hardness Analysis

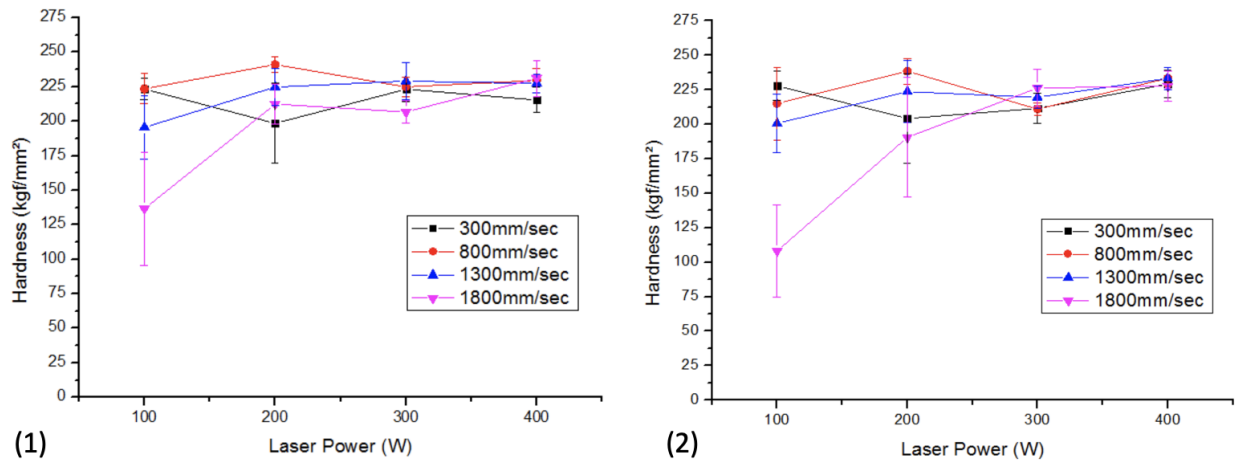


Figure 17. Change of Vickers hardness value as a function of laser power for each scanning speed in (1) scanning and (2) building directions.

Table 5. Vickers hardness results at different combinations of laser power (W) and scanning speed (mm/sec) for the scanning direction.

Scanning Direction	100W	200W	300W	400W
300mm/sec	223.29	198.49	223.22	215.41
800mm/sec	223.51	241.03	224.90	229.60
1300mm/sec	195.61	224.84	229.08	227.43
1800mm/sec	136.62	212.42	206.73	231.13

Table 6. Vickers hardness results at different combinations of laser power (W) and scanning speed (mm/sec) for the building direction.

Building Direction	100W	200W	300W	400W
300mm/sec	227.89	204.22	211.48	229.15
800mm/sec	215.02	238.37	210.96	233.30
1300mm/sec	200.62	223.63	219.51	233.24
1800mm/sec	108.21	190.55	226.24	227.61

Figure 17 illustrates the variation in hardness value (in both the scanning and building directions) as a function of laser power at each scanning speed. It is possible to observe a trend in both figures, which is that as laser power increases, hardness increases. The values for these hardnesses can be found in Tables 5 and 6. The highest value achieved

for the samples in the scanning direction was 241 ± 6 HV at 200 W of laser power and 800 mm/sec scanning speed, whereas the lowest value achieved was 136 ± 41 HV at 100 W of laser power and 1800 mm/sec scanning speed. With the exact same processing parameters that produce the maximum and minimum HV in the scanning direction, the samples in the building direction had a maximum value of 238 ± 9 HV and a minimum value of 108 ± 33 HV.

It is important to note that the uncertainty of low HV samples is significantly greater than that of high HV samples. During hardness testing, samples with minimal porosity exhibited indents that were nearly perfect squares and of comparable size. On the other hand, samples with higher porosities possessed varying indentation sizes. In addition to the varying indentation sizes, it was observed that few indents had square shapes. This shows that there is a direct correlation between hardness and porosity.

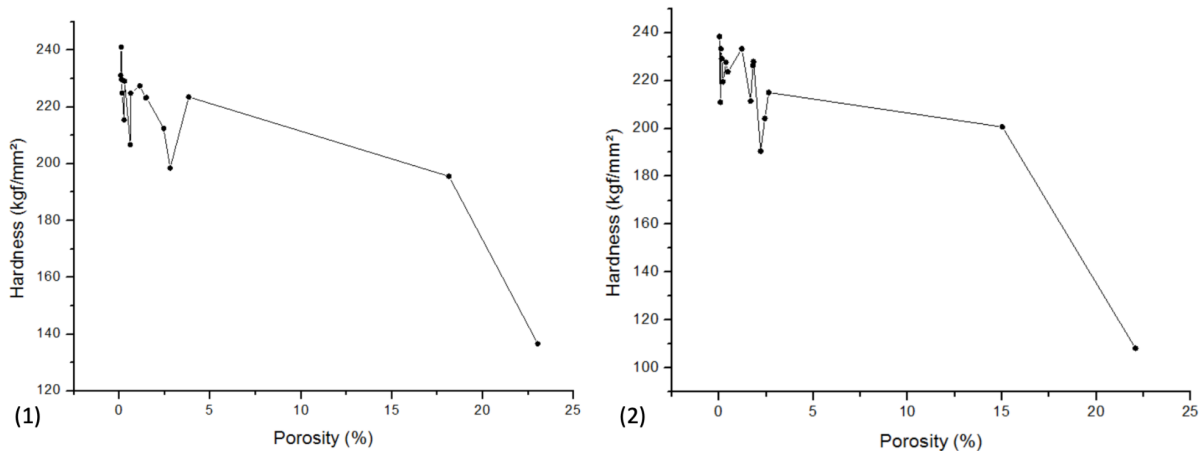


Figure 18. Vickers hardness as a function of porosity in the (1) scanning direction and in the (2) building direction.

At high laser powers, all samples exhibit increased hardness. As all high laser power samples have low porosity, Figure 18 is constructed to show the relationship between porosity and hardness in both scanning and building directions. It has been noticed that increasing porosity decreases the samples' hardness.

Figure 19 displays the sample hardness values in SD and BD. In nine of the samples, the measured hardness is greater in SD, and the average hardness of all samples is also greater in SD. W.M. Tucho et al. [49] determined the Vickers hardness values along SD and BD for SLM-manufactured SS-316L. In contrast to the findings of this study, the hardness of the BD samples was found to be greater. H. Li et al. [50] looked at the tribological performance of SLM-fabricated SS-316L and found that samples in the BD direction have slightly higher hardness values. However, both concluded that there was

no relationship between the hardness and the direction from which the samples were observed, which is the same conclusion derived in this research.

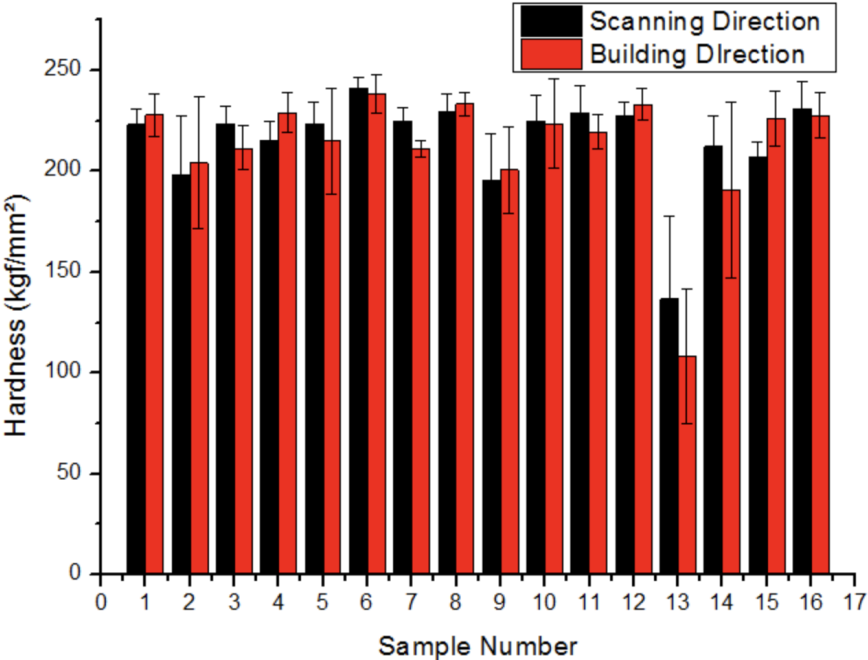


Figure 19. Vickers hardness measured on the surfaces along the scanning and building directions.

5.3 Functionally Gradient Porous Structure

Twelve samples of the proposed FGP structure were successfully manufactured, as shown in Figure 20 (1).

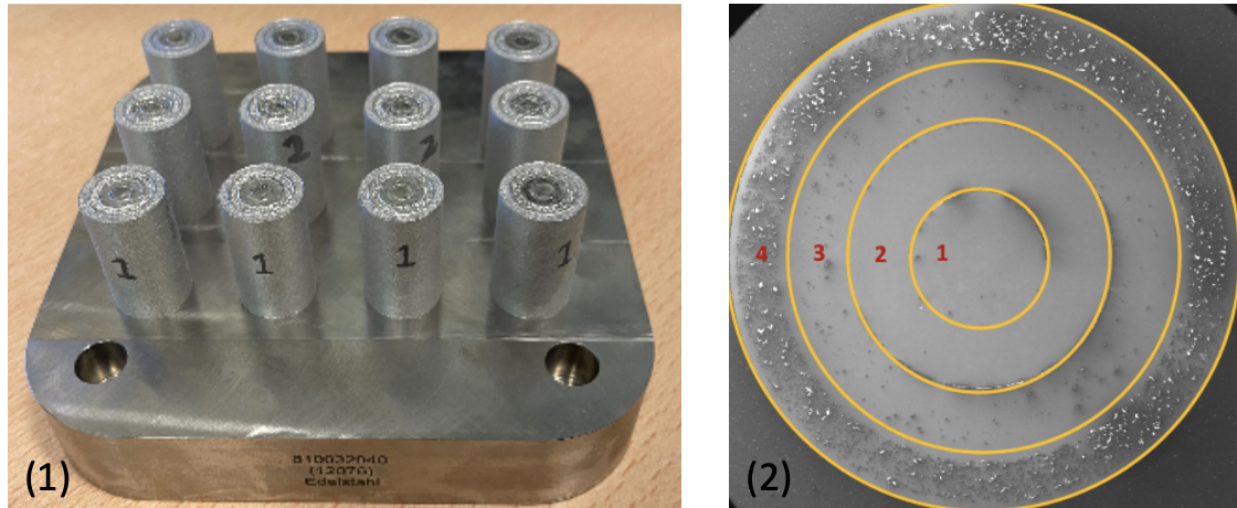


Figure 20. 12 FGP structure samples (1), and SEM image of a FGP structure (2).

Observing Figure 20 (2) reveals that the combination of different laser parameters, i.e., laser power and scanning speed, resulted in the formation of a properly fused solid structure. This indicates that the FGP structures could be manufactured with varying laser parameters within a single component. Consequently, the hypothesis formulated in Section 4.5, "Proposal of Functionally Gradient Porous Structure," is demonstrated to be accurate.

Due to time constraints and a malfunctioning SLM printer, the available FGP structures do not accurately depict the bone structure, which is characterized by increasing porosity toward the center. Before beginning any characterizations, these samples were initially printed out to determine if proper fusion would occur when different scanning parameters were utilized on a single specimen. Initial plans called for the printing of FGP structures resembling the internal morphology of bone once porosity and hardness analyses were performed on 16 individual samples.

6 Conclusion

First, the porosity morphology and fraction of 16 samples were analyzed to determine the impact of the laser power and scanning speed on the melting and solidification mechanisms of SS-316L. Then, a FGP structure is manufactured as explained in Section 4.5, “Proposal of Functionally Gradient Porous Structure”.

6.1 Impact of Laser Parameters on Melting and Solidification Mechanisms

The results of the analysis revealed a clear impact of the laser power and scanning speed on the melting and solidification mechanisms of the SS-316L samples. As laser power increased, porosity decreased, whereas porosity increased with an increase in scanning speed. The highest porosity value of 23.03% was observed at 100W laser power and 1800mm/s scanning speed. Moreover, it was found that lower laser power and higher scanning speed led to higher porosities, accompanied by different types of pores such as entrapped gas, keyhole, and lack of fusion pores. Additionally, samples 2, 5, 9, and 13 were found to possess promising mean pore sizes for implant applications, as explained at the end of Section 5.1, “Porosity Analysis”. Furthermore, a negative correlation was observed between the porosity and hardness of the manufactured samples. Finally, neither porosity nor hardness were found to be affected by the sample direction (building direction or scanning direction).

6.2 Proposed FGP Structure

SLM is currently being studied for making lattice-based porous structures. Designing lattice-based porous structures with the desired porosities is already a challenging task in the scientific domain. Designing lattice based gradient porous structures is even a harder task to complete. *This work gives new direction for implant manufacturing industries as well as researchers by showing that it is possible to develop gradient porous structures by changing laser parameters in a single component. This work can eliminate the complicated design steps for making gradient porous structures. This simplifies the manufacturing of gradient porous structures, providing new avenues for researchers, implant manufacturing industries, or any other industry that can benefit from FGP structures.*

6.3 Future Research

For future research, it is recommended to study the compressive deformation behavior of the SLM-produced FGP structures and compare this behavior to the actual human bones to reveal how closely the samples mimic the bone's compressive deformation behavior. Additionally, the permeability of the manufactured FGP structures should be determined, which would provide insight into how well the samples would mimic the bone in terms of proliferation, cell adhesion, and bone ingrowth.

7 References

- [1] M. Attaran, "[The rise of 3-D printing: The advantages of additive manufacturing over traditional manufacturing.](#)" Business Horizons, vol. 60, no. 5, pp. 677–688, 2017.
- [2] M. Gebler, A. J. M. Schoot Uiterkamp, and C. Visser, "[A global sustainability perspective on 3D printing technologies.](#)" Energy Policy, vol. 74, pp. 158–167, 2014.
- [3] H. Bikas, P. Stavropoulos, and G. Chryssolouris, "[Additive manufacturing methods and modelling approaches: A critical review.](#)" The International Journal of Advanced Manufacturing Technology, vol. 83, no. 1-4, pp. 389–405, 2015.
- [4] F. Caltanissetta, G. Dreifus, A. J. Hart, and B. M. Colosimo, "[In-situ monitoring of material extrusion processes via thermal video imaging with application to Big Area Additive Manufacturing \(BAAM\).](#)" Additive Manufacturing, vol. 58, p. 102995, 2022.
- [5] Y. L. Yap, C. Wang, S. L. Sing, V. Dikshit, W. Y. Yeong, and J. Wei, "[Material Jetting Additive Manufacturing: An experimental study using designed metrological benchmarks.](#)" Precision Engineering, vol. 50, pp. 275–285, 2017.
- [6] S. Sahoo and K. Chou, "[Phase-field simulation of microstructure evolution of ti–6al–4v in electron beam additive manufacturing process.](#)" Additive Manufacturing, vol. 9, pp. 14–24, 2016.
- [7] S. Yusuf, Y. Chen, R. Boardman, S. Yang, and N. Gao, "[Investigation on porosity and microhardness of 316L stainless steel fabricated by selective laser melting.](#)" Metals, vol. 7, no. 2, p. 64, 2017.
- [8] S. Waqar, Q. Sun, J. Liu, K. Guo, and J. Sun, "[Numerical investigation of thermal behavior and melt pool morphology in multi-track multi-layer selective laser melting of the 316L Steel.](#)" The International Journal of Advanced Manufacturing Technology, vol. 112, no. 3-4, pp. 879–895, 2020.
- [9] P. Ashwath, M. A. Xavier, A. Batako, P. Jeyapandiarajan, and J. Joel, "[Selective laser melting of Al–Si–10MG alloy: Microstructural studies and Mechanical Properties Assessment.](#)" Journal of Materials Research and Technology, vol. 17, pp. 2249–2258, 2022.
- [10] L. Jiao, Z. Chua, S. Moon, J. Song, G. Bi, and H. Zheng, "[Femtosecond laser produced hydrophobic hierarchical structures on additive manufacturing parts.](#)" Nanomaterials, vol. 8, no. 8, p. 601, 2018.
- [11] N. Read, W. Wang, K. Essa, and M. M. Attallah, "[Selective laser melting of als10mg alloy: Process optimisation and Mechanical Properties Development.](#)" Materials & Design (1980-2015), vol. 65, pp. 417–424, 2015.
- [12] S. Leuders, M. Thöne, A. Riemer, T. Niendorf, T. Tröster, H. A. Richard, and H. J. Maier, "[On the mechanical behaviour of titanium alloy TiAl6V4 manufactured by](#)

[selective laser melting: Fatigue resistance and crack growth performance.](#)” International Journal of Fatigue, vol. 48, pp. 300–307, 2013.

[13] N. T. Aboulkhair, I. Maskery, C. Tuck, I. Ashcroft, and N. M. Everitt, “[Improving the fatigue behaviour of a selectively laser melted aluminium alloy: Influence of heat treatment and surface quality.](#)” Materials & Design, vol. 104, pp. 174–182, 2016.

[14] M. Brandt, S. J. Sun, M. Leary, S. Feih, J. Elambasseril, and Q. C. Liu, “[High-value SLM Aerospace Components: From design to manufacture.](#)” Advanced Materials Research, vol. 633, pp. 135–147, 2013.

[15] M. Seabra, J. Azevedo, A. Araújo, L. Reis, E. Pinto, N. Alves, R. Santos, and J. Pedro Mortágua, “[Selective Laser Melting \(SLM\) and topology optimization for Lighter Aerospace Componentes.](#)” Procedia Structural Integrity, vol. 1, pp. 289–296, 2016.

[16] M. Bici, S. Brischetto, F. Campana, C. G. Ferro, C. Seclì, S. Varetto, P. Maggiore, and A. Mazza, “[Development of a multifunctional panel for aerospace use through SLM additive manufacturing.](#)” Procedia CIRP, vol. 67, pp. 215–220, 2018.

[17] S. G. Sarvankar and S. N. Yewale, “[Additive Manufacturing in Automobile Industry.](#)” INTERNATIONAL JOURNAL OF RESEARCH IN AERONAUTICAL AND MECHANICAL, vol. 7, pp. 01–10, Apr. 2019.

[18] R. Khandelwal, “[Additive Manufacturing in the Automotive Industry.](#)” International Research Journal of Engineering and Technology (IRJET), vol. 07, pp. 2008–2014, Aug. 2020.

[19] J. Pieklo and A. Garbacz-Klempka, “[Use of Selective Laser Melting \(SLM\) as a Replacement for Pressure Die Casting Technology for the Production of Automotive Casting.](#)” Archives of Foundry Engineering, vol. 21, no. 2, pp. 9–16, 2021.

[20] S. Ferraris and S. Spriano, “[Porous titanium by additive manufacturing: A focus on surfaces for bone integration.](#)” Metals, vol. 11, no. 9, p. 1343, 2021.

[21] A. Gebhardt, F.-M. Schmidt, J.-S. Hötter, W. Sokalla, and P. Sokalla, “[Additive manufacturing by selective laser melting the realizer desktop machine and its application for the Dental Industry.](#)” *Physics Procedia*, vol. 5, pp. 543–549, 2010.

[22] E. Wycisk, C. Emmelmann, S. Siddique, and F. Walther, “[High cycle fatigue \(HCF\) performance of ti-6al-4v alloy processed by selective laser melting.](#)” Advanced Materials Research, vol. 816-817, pp. 134–139, 2013.

[23] “Home,” English. [Online]. Available: <https://wzppgi.com/difference-between-ss316-and-ss316/>. [Accessed: 05-Feb-2023].

[24] S. Mirzababaei and S. Pasebani, “[A review on binder jet additive manufacturing of 316L stainless steel.](#)” Journal of Manufacturing and Materials Processing, vol. 3, no. 3, p. 82, 2019.

- [25] O. Hussain, S. Saleem, and B. Ahmad, "[Implant materials for knee and Hip Joint Replacement: A review from the Tribological Perspective.](#)" IOP Conference Series: Materials Science and Engineering, vol. 561, no. 1, p. 012007, 2019.
- [26] M. Z. Ibrahim, A. A. D. Sarhan, T. Y. Kuo, F. Yusof, M. Hamdi, and T. M. Lee, "[Developing a new laser clad FeCrMoCB metallic glass layer on nickel-free stainless-steel as a potential superior wear-resistant coating for joint replacement implants.](#)" Surface and Coatings Technology, vol. 392, p. 125755, 2020.
- [27] Mohandoss, S., et al. "[Surface Modification of 316L Stainless Steel dental implants by Novel Bioinert Nano Zirconia coating.](#)" Trends in Biomaterials and Artificial Organs, vol. 34, no. 3, July 2020, pp. 100+.
- [28] K. Larrimore, "What is food-grade stainless steel?," Hose Coupling Industry Blog. [Online]. Available: <https://blog.dixonvalve.com/what-is-food-grade-stainless-steel>. [Accessed: 05-Feb-2023].
- [29] M. Manager, "Stainless steel uses in food industry: Stainless Steel Blog," Stainless Steel Blog | THE OFFICIAL BLOG OF AMBICA STEELS LTD. [Online]. Available: <https://www.ambicasteels.com/blog/stainless-steel-in-food-industry/>. [Accessed: 05-Feb-2023].
- [30] G. Jena, B. Anandkumar, S. Sofia, R. P. George, and J. Philip, "[Fabrication of silanized go hybrid coating on 316L SS with enhanced corrosion resistance and antibacterial properties for marine applications.](#)" Surface and Coatings Technology, vol. 402, p. 126295, 2020.
- [31] S. Gupta, D. Singh, A. Yadav, S. Jain, and B. Pratap, "[A comparative study of 5083 aluminium alloy and 316L stainless steel for shipbuilding material.](#)" Materials Today: Proceedings, vol. 28, pp. 2358–2363, 2020.
- [32] L. Civmats Co., "316L stainless steel-introduction, applications, Data Sheet," civmats.com. [Online]. Available: <https://www.civmats.com/grades/GRADES-316L.HTML>. [Accessed: 05-Feb-2023].
- [33] S. Wang, J. Li, Y. Cao, B. Gao, Q. Mao, and Y. Li, "[Thermal stability and tensile property of 316L stainless steel with heterogeneous lamella structure.](#)" Vacuum, vol. 152, pp. 261–264, 2018.
- [34] M. Tilton, G. S. Lewis, and G. P. Manogharan, "[Additive Manufacturing of orthopedic implants.](#)" Orthopedic Biomaterials, pp. 21–55, 2018.
- [35] H. Lei, T. Yi, H. Fan, X. Pei, L. Wu, F. Xing, M. Li, L. Liu, C. Zhou, Y. Fan, and X. Zhang, "[Customized additive manufacturing of porous ti6al4v scaffold with micro-topological structures to regulate cell behavior in bone tissue engineering.](#)" Materials Science and Engineering: C, vol. 120, p. 111789, 2021.

- [36] D. Mahmoud, K. S. Al-Rubaie, and M. A. Elbestawi, "[The influence of selective laser melting defects on the fatigue properties of ti6al4v porosity graded gyroids for Bone Implants.](#)" International Journal of Mechanical Sciences, vol. 193, p. 106180, 2021.
- [37] J. J. Dunkley, "[Metal powder atomisation methods for modern manufacturing.](#)" Johnson Matthey Technology Review, vol. 63, no. 3, pp. 226–232, 2019.
- [38] L. Achelis and V. Uhlenwinkel, "[Characterisation of metal powders generated by a pressure-gas-atomiser.](#)" Materials Science and Engineering: A, vol. 477, no. 1-2, pp. 15–20, 2008.
- [39] C. Additive, "Metal Powders & Solutions for AM," Carpenter Additive. [Online]. Available: <https://www.carpenteradditive.com/>. [Accessed: 05-Feb-2023].
- [40] D. H. Kumar and A. S. Reddy, "[STUDY OF MECHANICAL BEHAVIOR IN AUSTENITIC STAINLESS STEEL 316 LN WELDED JOINTS.](#)" Internationalk Journal of Mechanical Engineering and Robotics Research, vol. 2, no. 1, pp. 37–56, Jan. 2013.
- [41] J.-M. Schneider, M. Bigerelle, and A. Iost, "[Statistical analysis of the Vickers hardness.](#)" Materials Science and Engineering: A, vol. 262, no. 1-2, pp. 256–263, 1999.
- [42] A. Sola and A. Nouri, "[Microstructural porosity in Additive Manufacturing: The formation and detection of pores in metal parts fabricated by Powder Bed Fusion.](#)" Journal of Advanced Manufacturing and Processing, vol. 1, no. 3, 2019.
- [43] T. Wang, Y. Wang, C. Chen, and H. Zhu, "[Relationships between the characteristics of porosity, melt pool and process parameters in laser powder bed fusion al Zn alloy.](#)" Journal of Manufacturing Processes, vol. 68, pp. 1236–1244, 2021.
- [44] J.-N. Zhu, E. Borisov, X. Liang, E. Farber, M. J. M. Hermans, and V. A. Popovich, "[Predictive analytical modelling and experimental validation of processing maps in additive manufacturing of Nitinol Alloys.](#)" Additive Manufacturing, vol. 38, p. 101802, 2021.
- [45] S. Yusuf, Y. Chen, R. Boardman, S. Yang, and N. Gao, "[Investigation on porosity and microhardness of 316L stainless steel fabricated by selective laser melting.](#)" Metals, vol. 7, no. 2, p. 64, 2017.
- [46] S. Shrestha and K. Chou, "[Formation of keyhole and lack of fusion pores during the laser powder bed fusion process.](#)" Manufacturing Letters, vol. 32, pp. 19–23, 2022.
- [47] C. M. Murphy, M. G. Haugh, and F. J. O'Brien, "[The effect of mean pore size on cell attachment, proliferation and migration in collagen–glycosaminoglycan scaffolds for bone tissue engineering.](#)" Biomaterials, vol. 31, no. 3, pp. 461–466, 2010.
- [48] C. M. Murphy and F. J. O'Brien, "[Understanding the effect of mean pore size on cell activity in collagen-glycosaminoglycan scaffolds.](#)" Cell Adhesion & Migration, vol. 4, no. 3, pp. 377–381, 2010.

- [49] W. M. Tucho, V. H. Lysne, H. Austbø, A. Sjolyst-Kverneland, and V. Hansen, "[Investigation of effects of process parameters on microstructure and hardness of SLM manufactured SS316L](#)," Journal of Alloys and Compounds, vol. 740, pp. 910–925, 2018.
- [50] H. Li, M. Ramezani, M. Li, C. Ma, and J. Wang, "[Tribological performance of selective laser melted 316L stainless steel](#)," Tribology International, vol. 128, pp. 121–129, 2018.